Size-dependent protein segregation creates a spatial switch for Notch and APP signaling

Minsuk Kwak[1,2,3,4,5,6,*], Kaden M. Southard[1,2,*], Nam Hyeong Kim[1,2,3,6], Ramu Gopalappa[4,8], Woon Ryoung Kim[1,2,3], Minji An[4,5], Hyun Jung Lee[1,2,3], Justin Farlow[2], Anastasios Georgakopoulos[9], Nikolaos K. Robakis[9], Daeha Seo[10], Hyeong Bum Kim[4,5,8,11,12], Yong Ho Kim[6,7], Jinwoo Cheon[4,5,13], Zev J. Gartner[2,14,†], Young-wook Jun[1,2,3,4,5†]

[1]Department of Otolaryngology, University of California, San Francisco, CA, USA

[2]Department of Pharmaceutical Chemistry, University of California, San Francisco, CA, USA

[3]Helen Diller Family Cancer Comprehensive Center (HDFCCC), University of California, San Francisco, CA, USA

[4]Center for Nanomedicine, Institute for Basic Science (IBS), Seoul, Republic of Korea

[5]Graduate Program of Nano Biomedical Engineering (Nano BME), Advanced Science Institute, Yonsei University, Seoul, Republic of Korea

[6]SKKU Advanced Institute of Nanotechnology (SAINT), Sungkyunkwan University, Suwon, Republic of Korea

[7]Department of Biomedical Engineering, Sungkyunkwan University, Suwon, Republic of Korea

[8]Department of Pharmacology, Yonsei University College of Medicine, Seoul, Republic of Korea

[9]Department of Psychiatry and Neuroscience, Icahn School of Medicine at Mount Sinai, New York, USA

[10]Department of Emerging Materials Science, DGIST, Daegu, Republic of Korea

[11]Brain Korea 21 Plus Project, Yonsei University College of Medicine, Seoul, Republic of Korea

[12]Severance Biomedical Science Institute, Yonsei University College of Medicine, Seoul, Republic of Korea

[13]Department of Chemistry, Yonsei University, Seoul, Republic of Korea

[14]Chan Zuckerberg Biohub, University of California San Francisco, CA, USA

*These authors contributed equally.

[†]Correspondence should be addressed to Z.J.G. (zev.gartner@ucsf.edu) or Y.J. (young-wook.jun@ucsf.edu).

Aberrant cleavage of Notch and amyloid precursor proteins (APPs) by γ-secretase is implicated in numerous diseases, but how cleavage is regulated in space and time is unclear. Here, we report that cadherin-based adherens junctions (cadAJs) are sites of high cell-surface γ-secretase activity, while simultaneously excluding these γ-secretase substrates by a size-dependent mechanism, prohibiting enzyme-substrate interactions. Upon activation, Notch and APP undergo drastic spatial rearrangements to cadAJs, concentrating them with γ-secretase, wherein they are further processed for downstream signaling. Spatial mutation by decreasing (or increasing) the size of Notch extracellular domain promotes (or inhibits) signaling, respectively. Dysregulation of this spatial switch also promotes formation of more amyloidogenic Aβ. Therefore, cadAJs creates distinct biochemical compartments regulating signaling events involving γ-secretase and prevent pathogenic activation of its substrates.

Notch is a highly conserved mediator for contact-dependent cell-cell communication, which orchestrates diverse functions in metazoans (*1*, *2*). Tight control of Notch signal activation is essential for many developmental processes, while dysregulation of Notch activation can cause severe disease including developmental, neurological, and immunological disorders and cancer (*1-4*). Accordingly, to enable precise signal regulation, receptor activation occurs through multiple steps, independently gated by chemical (e.g., ligand-receptor interactions, posttranslational modifications) and mechanical cues (*1*, *2*, *5-9*). However, many signaling processes involving physical contact between two cells – so called juxtacrine signaling processes – are also regulated by spatial cues (*10-12*). As exemplified by the kinetic segregation model in immune cells (*10*, *12*, *13*), spatial rearrangements of these signaling molecules modify their physical and biochemical environments to facilitate receptor activation. Notch, which also mediates signal exchange by physical contact, is subjected to similar structural and spatial rearrangements (*14*, *15*). To test whether Notch signaling is regulated by these spatial rearrangements, we investigated the spatial dynamics of Notch and its signaling partners at cellular interfaces. Specifically, we focused on four key signaling molecules – Notch, delta-like ligand 1 (Dll1), ADAM 10, and γ-secretase, relative to cadherin-based adherens junctions (cadAJs); the cell-cell adhesions that initiate many structural and spatial changes by bringing and holding the membranes together (*16-18*) (**Fig. 1A**).

CadAJs segregate Notch from γ-secretase, preventing interactions

To map the distribution of Notch signaling components, we generated a series of U2OS cells expressing recombinant Notch1, Dll1, and/or epithelial cadherin (E-cadherin, Ecad) proteins. To facilitate the imaging of these proteins, we fused them with self-labeling tags (SNAP or Halo-tags) and/or fluorescent proteins (EGFP or mCherry) at the N- or C-termini, respectively (**Table S1**). The endogenous Notch processing enzymes (*i.e.* ADAM 10, and γ-secretase) were immunostained and then imaged by confocal microscopy. With the exception of ADAM 10 which exhibited no preferential distribution relative to cadAJs (**fig. S1A**), all other proteins exhibited cadAJ-dependent localization (**Fig. 1, B and C**). γ-secretase (visualized by staining with an anti-presenilin-1 antibody) was strongly enriched at the cadAJs with negligible non-junctional membrane signal (**Fig. 1, B and C, and fig. S1, B and C**) (*19*). In contrast, both Notch and Dll1 were excluded from cadAJs (**Fig. 1, B and C**) and consequentially γ-secretase (**fig. S2, A and B**). Notch exclusion from cadAJs was observed in multiple contexts, including different cadherin types, cell types, and cell polarization states (**fig. S3**). Quantitative analysis using the Manders' overlap coefficient to calculate fractional overlap with E-cadherin also confirmed the enrichment of γ-secretase (0.85 ± 0.21) at cadAJs and the exclusion of Notch (0.24 ± 0.19) and Dll1 (0.26 ± 0.18) from cadAJs (**fig. S2, C and D**). These observations suggest two mechanisms by which cadAJs might influence Notch signaling: first, cadAJs recruit γ-secretase; second, cadAJs segregate Notch ligands and receptors from γ-secretase to prevent their interactions.

To interrogate how cadAJs drive the spatial segregation of the enzyme (*i.e.* γ-secretase) and substrate (*i.e.* Notch) pair, we employed our recently developed single-cell perturbation tool, mechanogenetics, where magnetofluorescent nanoparticles (MFNs) control the location and mechanical loading of targeted receptors hence cell signaling (*9*, *20*, *21*). Specifically, we clustered E-cadherin using mechanogenetics to generate artificial cadAJs that recapitulate the functional and signaling roles of native cadAJs (*9*, *20*, *21*) (**Fig. 1, D and E**; See Methods for details). We then monitored the consequence of cadAJ formation on the spatial distributions of γ-secretase, Notch, and associated proteins (e.g. Flotillin-1, Flot1) relative to the artificial cadAJ (**Fig. 1, F and G**). Consistent with the native cell-cell cadAJs, γ-secretase was localized at the artificial cadAJ (**Fig. 1F and fig. S4**). We also observed colocalization of Flot1, a protein enriched in spatially discrete and ordered membrane microdomains at the artificial cadAJs (*16-18*) (**Fig. 1F and fig. S4**). This observation, along with analysis of native cell-cell junctions (**fig. S5**), molecular dynamics (MD) simulation (**fig. S6, A to C**), and cholesterol depletion experiments (**fig. S6D**), suggests that the cadAJs recruit and stabilize γ-secretase through a common spatially discrete and ordered membrane microdomains (for more discussion, see **Supplementary Text**).

Surprisingly, we observed an intense Notch signal at the artificial cadAJ (**Fig. 1G and fig. S7**), in contrast to the depleted Notch signal at native cell-cell cadAJs (**Fig. 1, A to C**). The extraordinarily large size (extended length = 136 nm) of the Notch extracellular domain (NECD) (*22*) suggested a potential explanation for these contradicting observations. Specifically, Notch could be excluded from cadAJs due to the NECD size greatly exceeding the narrow intermembrane cleft created by native cadAJs (20 nm)(*17*, *23*). On the other hand, artificial cadAJs generated by MFNs are free of membrane juxtaposition and hence allow for Notch diffusion and accumulation, presumably through its association with γ-secretase or other components of the membrane microdomains (*24*). These observations fit a model wherein the size-based physical constraint caused by cell-cell cadAJs segregates Notch from γ-secretase, preventing interactions that would otherwise serve to colocalize and concentrate the enzyme-substrate pair.

Size-dependent segregation choreographs the Notch proteolytic sequence

Upon activation by juxtacrine ligand-receptor interactions, Notch is processed by ADAM 10/17 (S2 cleavage) and then by γ-secretase (S3 cleavage), sequentially (*1*, *2*). Since each of proteolytic events leads to a dramatic reduction in the size of NECD, we investigated how the size changes during activation correlate with its spatial distribution. We plated U2OS cells co-expressing SNAP-N^{FL}-mCherry and Ecad-GFP on a Dll4-coated substrate to trigger Notch activation. Cells were also treated with TAPI2 (an ADAM 10/17 inhibitor which stabilizes full-length Notch) or DAPT (a γ-secretase inhibitor that stabilizes the S2-cleaved Notch having a minimal extracellular domain) to capture Notch intermediates (**Fig. 2A**). To quantify the spatial redistribution of each Notch intermediate relative to the cadAJ, we measured the average mCherry fluorescence signal inside (I_{IN}) and outside (I_{OUT}) of the cadAJ and

estimated an enrichment ratio (I_{IN}/I_{OUT}, See Supplementary Information). An intensity ratio of 1 represents no cadAJ-dependent distribution as validated with DiI dyes (I_{IN}/I_{OUT} = 1.07, **Fig. 2C and fig. S8A**), and values less than or greater than 1 represent exclusion from or enrichment within cadAJs, respectively. With TAPI2, we observed minimal mCherry fluorescence signal from cadAJs (I_{IN}/I_{OUT} = 0.50, **Fig. 2, B**(ii) **and C**(ii)), indicating that the ligand-receptor interaction did not alter the spatial distribution of Notch before S2 cleavage. In contrast, when TAPI2 was removed to activate S2 cleavage and DAPT was added to inhibit S3 cleavage, we observed strong enrichment of the mCherry signal at cadAJs (I_{IN}/I_{OUT} = 2.14, **Fig. 2, B**(iii) **and C**(iii)), indicative of relocalization and concentration of the Notch extracellular domain truncation (NEXT), the product of S2 cleavage, into cadAJs. When γ-secretase activity was rescued by washing out DAPT, the initially intense mCherry signal at cadAJs gradually disappeared (**Fig. 2, B**(iv) **and C**(iv)**, and fig. S8, B and C**), presumably corresponding to release of Notch intracellular domain (NICD) from the membrane. These results suggest a role for the size-dependent protein segregation as a spatial switch that regulates the distribution of Notch intermediates, thereby choreographing the sequential steps in Notch proteolysis. According to this model, the mass of NECD poses a physical constraint preventing entry of Notch to the narrow space between membranes in the cadAJ cleft where γ-secretase is localized. Hence, γ-secretase cannot process the full-length Notch before S2 cleavage. Following S2 cleavage, removal of NECD relieves the physical constraint, allowing Notch to enter into the cadAJ cleft. This facilitates a productive Notch-γ-secretase interaction (*24*), S3 cleavage, and then downstream signaling.

To explore how size-dependent segregation controls Notch signaling, we first generated a series of U2OS cell lines stably expressing Notch variants with different truncation lengths: a partial deletion of the EGF repeats (NΔEGF$_{1\text{-}25}$, approximate height: 48 nm), complete deletion of the EGF repeats but retention of negative regulatory region (NΔEGF, approximate height: 10 nm), and a complete removal of NECD (NEXT, approximate height: 4 nm) (**Fig. 2D**). We fused these Notch variants with SNAP- and mCherry-tags at their N- and C-termini, to differentially image the extracellular and intracellular domains. All cells were treated with TAPI2 and DAPT to prevent any potential proteolysis of the variants. Consistent with predictions based on size-dependent protein segregation, NΔEGF$_{1\text{-}25}$, the Notch variant with an ECD taller than the height of the intermembrane cadAJ cleft, was excluded from cadAJs (I_{IN}/I_{OUT} = 0.57) (**Fig. 2, E and F**). NEXT with an ECD smaller than the junctional height was enriched at cadAJs (I_{IN}/I_{OUT} = 2.39) (**Fig. 2, E and F**). Interestingly, we observed binary localizations of NΔEGF (intermediate height) relative to cadAJs, with a mean I_{IN}/I_{OUT} value of 1.32 (**Fig. 2, E and F**). Some cadAJs displayed NΔEGF enrichment (**Fig. 2, E**(bottom left) **and F**(right)), consistent with the size-based prediction. Meanwhile, other cadAJs excluded NΔEGF (**Fig. 2, E**(bottom right) **and F**(right)). Considering the fact that cadherin cluster densities within cadAJs vary with the size, type, and degree of junction maturation (*25*, *26*) and that the glycosylated negative regulatory region domain (*6*) is susceptible to steric crowding, this unanticipated exclusion might result from a lateral crowding effect in high-density cadAJs.

We then investigated the functional consequences of NΔEGF relocalization to cadAJs by measuring the impact on downstream signaling process. Focusing on the subset of cadAJs showing strong enrichment for Notch signal, we inferred γ-secretase activity by measuring the changes in extracellular SNAP (labeled with SNAP surface dye) and intracellular mCherry fluorescence signals of NΔEGF after DAPT removal while maintaining TAPI2 concentration. This construct has different fluorescence markers on the extracellular and intracellular domains of the protein, allowing us to differentially map the S2 and S3 cleavage events of the construct. While SNAP fluorescence signal remained strong, the mCherry signal at the cadAJ was negligible (**Fig. 3A**). Similarly, colocalization analysis of multiple cadAJs using Pearson correlation coefficients showed more significant signal reduction in the mCherry channel than in SNAP, indicating selective release of NICD from cadAJs (**Fig. 3B**). We measured the kinetics of S3 processing by tracking mCherry intensity at the cadAJ in single cells. Initially intense mCherry signals (average I_{IN}/I_{OUT} = 2.89 ± 1.15) rapidly dissipated within the first 2 hours following DAPT removal (average I_{IN}/I_{OUT} = 0.81 ± 0.42), reaching a plateau at 4 hours (I_{IN}/I_{OUT} = 0.65 ± 0.14) **(Fig. 3, C and D, and fig. S9, A and B**). Removing DAPT did not elicit a significant reduction in mCherry signal intensity from the non-cadAJ membrane, indicating that the S3 cleavage activity was strongly localized at the cadAJ (**fig. S9C**). To confirm that the observed decrease in mCherry signal at the cadAJ corresponds to the S3 cleavage, we performed western blot analysis of the cells expressing the Notch variants. We cultured cells with TAPI2 to decouple γ-secretase processing from S2 cleavage, and measured cleaved NICD levels by immunoblotting with Notch anti-V1744 antibodies. Cells expressing N^{FL} or $N\Delta EGF_{1\text{-}25}$ resulted in no or minimal NICD, respectively (**Fig. 3, E and F**). Whereas, cells expressing NΔEGF produced a significant amount of NICD (**Fig. 3, E and F**). Cells expressing NEXT exhibited the highest NICD production, about a 4-fold increase compared with that of NΔEGF (**Fig. 3, E and F**). The observed NICD production levels were proportional to the enrichment ratio (I_{IN}/I_{OUT}) of the Notch variants at cadAJs, suggesting the essential role of size-dependent protein segregation as a spatial switch that controls Notch activation. Additionally, the substantial NICD production from the cells expressing NΔEGF indicates that, when localized together, γ-secretase can process Notch, bypassing S2 cleavage. Ligand-independent activation of Notch receptors with an intact S2 site was observed previously in Notch truncation variants or synNotch constructs (*27-29*), but the mechanism of this activation has been unclear so far. Our observations support the notion that colocalization of Notch with γ-secretase is sufficient to trigger S3 proteolysis and signaling.

Spatial mutation alters Notch signaling

Prevailing models of Notch proteolysis by γ-secretase are based on the notion that S2-cleavage of Notch serves to potentiate the cleavage by modifying the molecular interface at the enzyme-substrate pair (*30*, *31*). For example, it has been suggested that γ-secretase selectively recognizes S2-cleaved Notch (*i.e.,* NEXT) through hydrogen bonding between a glutamate residue in nicastrin and the new N-

terminus of NEXT(*30*). Another model proposed that S2 cleavage serves to reduce steric repulsion between nicastrin and NECD, strengthening their interaction (*31*). However, another key feature of S2 cleavage is that it generates a smaller molecular intermediate that can uniquely access cadAJs, thereby colocalizing Notch with γ-secretase and significantly increasing its concentration near the enzyme active site. This suggests a third model, wherein γ-secretase activity on full length Notch and its intermediates is blocked by maintaining Notch concentrations below the K_M for γ-secretase through spatial segregation.

To explicitly test the effect of Notch spatial localization relative to cadAJs and γ-secretase on the signaling, we designed two experiments that induce spatial mutation of Notch. First, we employed a DNA-mediated crosslinking strategy to enhance NΔEGF – a Notch variant that exhibited binary localizations relative to cadAJs and relatively low Notch activation – enrichment at the cadAJ. We generated cells co-expressing SNAP-NΔEGF-mCherry and Halo-Ecad-GFP, and treated the cells with complementary BG- and chloroalkane-modified oligonucleotides in the presence of TAPI2 and DAPT (**Fig. 4A**). Notch-E-cadherin heterodimers were formed efficiently as evidenced by the appearance of a higher molecular weight band corresponding to the DNA-linked complex on western blots (**fig. S10A**). Compared to untreated cells (I_{IN}/I_{OUT} = 1.32 ± 1.06), we observed further enrichment of NΔEGF at cadAJs in the presence of DNA crosslinking (I_{IN}/I_{OUT} = 1.89 ± 0.91) (**Fig. 4B**). We then maintained cells in TAPI2 but removed DAPT to allow S3 cleavage. We observed decreases in mCherry signal at cadAJs after DAPT removal, indicating efficient S3 cleavage without S2 cleavage (**fig. S10, B to D**). Interestingly, in western blots, we observed increased V1744-terminated NICD levels from the cells treated with DNA crosslinkers, compared with the untreated control (**Fig. 4C**). There results suggest that new molecular interfaces produced by mechanical activation and S2 cleavage are not necessary when γ-secretase is concentrated with its substrate. Considering that DNA crosslinking (molecular weight = 21.4 kD) increases the ECD size of NΔEGF, the observed increase in NICD production cannot be explained by the nicastrin-induced steric repulsion model. Hence, we concluded the result that increased concentration of the NΔEGF at cadAJs facilitated its interaction with γ-secretase and promoted S3 cleavage.

To further test the importance of size-dependent spatial segregation, we induced spatial mutation of NEXT (*i.e.* the Notch variant that showed the strongest enrichment at the cadAJ and activation) by chemically conjugating it with macromolecules. Specifically, we conjugated BG-modified polymers and proteins, to the extracellular SNAP tag (4.0 nm) of the variant via BG-SNAP chemistry (**Fig. 4D**). Grafting of these macromolecular pendants onto NEXT increases the size of the Notch construct but does not modify the N-terminal amine accessibility for hydrogen bonding with nicastrin. To interrogate the size-dependent spatial mutation of NEXT systematically, we used a series of pendants with different hydrodynamic sizes, that includes polyethylene glycol with an average molecular weight of 3.4 kD (PEG3.4k, 2.5 nm), branched PEG20k (*b*PEG20k, 4.0 nm), linear PEG20k (ℓPEG20k, 8.0 nm), DNA-streptavidin conjugates (DNA-stv, 9.5 nm), and human immunoglobulin G (hIgG, 12 nm) (**Fig.**

4D and fig. S11A). In the presence of DAPT, we observed a size-dependent distribution of NEXT at the cadAJ, where the larger pendant resulted in a greater decrease in mCherry signal at the cadAJ. With pendants smaller than 5 nm (*i.e.* PEG3.4k and *b*PEG20*k*), NEXT remained enriched at the cadAJ with I_{IN}/I_{OUT} of 2.21 and 2.01, respectively (**Fig. 4, D and E**). When ℓPEG20k, DNA-stv, or hIgG were added, we observed binary localizations of NEXT that were enriched at or excluded from the cadAJs, with mean I_{IN}/I_{OUT} values of 1.06, 0.82, 0.98, respectively (**Fig. 4, D and E**). These observations were similar to the spatial behaviors of NΔEGF having a comparable ECD size, where only less dense cadAJs allowed Notch colocalization. We then examined the signaling consequences of each size-dependent spatial mutation of NEXT. Following S3 cleavage, NICD traffics to the nucleus, allowing us to measure nuclear mCherry signal as a proxy for Notch pathway activation. The PEG3.4k or *b*PEG20k addition did not significantly alter nuclear mCherry signal of NEXT, compared with cells with no pendant addition (**Fig. 4, F and G, and fig. S11B**). Conjugation of ℓPEG20k, DNA-stv (9.5 nm) resulted in substantial decrease in nuclear mCherry signal to 0.39 and 0.37, respectively (**Fig. 4, F and G, and fig. S11B**). hIgG addition slightly further suppressed nuclear mCherry signal to 0.27 (**Fig. 4, F and G, and fig. S11B**). Finally, we summarized the S3-cleaved NICD production of all Notch variants as a function of the Notch enrichment factor, I_{IN}/I_{OUT}, in **Fig. 4H**, clearly visualizing the spatial dependence of S3 cleavage.

The cadAJ-mediated spatial switch is indispensable for Notch signaling

Given the significant role of cadAJs in coordinating the spatial dynamics of Notch and γ-secretase, we next interrogated Notch signal activation in cells lacking cadAJs. To minimize physical contact between cells and hence cadAJ formation, we sparsely plated cells expressing SNAP-Notch-Gal4 (SNAP-N^{FL}-Gal4) receptors on a Dll4-coated substrate. We used a UAS-Gal4 reporter system that detects Notch activation with nuclear mCherry signal (*8*, *9*, *32*). After 16 hours from cell seeding, we measured the mCherry fluorescence in cells having no prior contact with other cells. For comparison, we also analyzed the mCherry signal in cells with robust cadAJs within high-density culture. While the cells with physical contacts with other cells exhibited robust increase in nuclear mCherry fluorescence signal, those without cell-cell contact elicited no increase in signal (**Fig. 5, A and B, and Movie S1**). Reestablishing the cadAJs by plating cells on a substrate coated with Ecad-Fc and Dll4-Fc rescued the Notch signaling of the solitary cells (**Fig. 5, A and C, and Movie S2**). These results support that cadAJs are required for Notch processing at the cell surface and downstream signaling. Critically, E-cadherin seems to function in this capacity in a manner that is independent of its role in mediating cell-cell contact. To further test this notion, we knocked out the gene encoding E-cadherin (CDH1) in the reporter cell line via CRISPR-Cas9, then plated the cells at high density on Dll4-Fc coated plates (**fig. S12, A to E**). Strikingly, E-cadherin knockout (Ecad-KO) resulted in abrogation of Notch activation even with robust cell-cell contact (**Fig. 5, D and E, and fig. S12F**). Reintroduction of plasmids encoding E-

cadherin or N-cadherin into Ecad-KO cells recovered Notch activation with substantial nuclear mCherry signal, confirming the indispensable role of cadAJs in Notch signaling (**Fig. 5, D and E, and fig. S12F**).

Size-dependent spatial dynamics and proteolysis of amyloid precursor proteins

The proteolysis processes of amyloid precursor protein (APP) plays a central role in amyloid beta (Aβ) pathology, which can cause failures in many organs such as brain, heart, kidney, and vasculatures (*33-36*). Interestingly, APP has a strikingly similar topology and proteolytic cleavage sequence to that of Notch. APP possesses a large ECD (> 20 nm) and is processed by α- or β-secretase and then γ-secretase (*33-35*). These characteristics motivated us to investigate the role of the size-dependent protein segregation in APP processing. We generated U2OS cells co-expressing APP-GFP and SNAP-N-cadherin (SNAP-Ncad) and monitored the cell surface spatial dynamics of APP intermediates relative to N-cadherin based AJs (NcadAJs) using proteolytic enzyme inhibitors. Similar to Notch, we found that APP was initially excluded from NcadAJs, diffused into the NcadAJs after the ECD shedding by α- or β-secretase, and then was processed by γ-secretase within it (**Fig. 5F**).

APP can be processed along two pathways by γ-secretase – one pathway occurs at the cell surface to generate more soluble isoforms including p3 or $A\beta_{40}$, the other pathway occurs internally to produce less soluble and pathogenic $A\beta_{42}$ (*33-35*). Given our previous observation that loss of cadAJs leads to a decrease in cell surface γ-secretase, we hypothesized that APP processing would be biased under these conditions towards $A\beta_{42}$. We tested this hypothesis by constructing U2OS cell lines lacking both E- and N-cadherins (cad-KO cells) using CRISPR-Cas9 (**fig. S13**). We then transfected plain U2OS cells or cad-KO cells with a plasmid encoding APP sequence and measured Aβ production by ELISA. Consistent with the hypothesis, cad-KO cells produced higher $A\beta_{42}$, the isoform prone to severe fibril aggregation, compared to cells with endogenous cadherin expression (**Fig. 5G**).

Discussion

Notch displays several unique features that are distinct from other juxtacrine receptors. For example, unlike classical receptor signaling, the Notch ligand-receptor interaction (chemical switch) is converted into intracellular signaling through a sequence of additional signaling switches acting by mechanical, enzymatic, and spatial mechanisms. These include unfolding of the negative regulatory region domain (mechanical switch), S2- and S3- cleavages (enzymatic switch), and finally translocation of the NICD from the cell membrane to the nucleus (spatial switch) (*1*, *2*). Our study reveals that Notch additionally integrates a spatial switch at the cell surface to tightly choreograph the enzymatic cleavage sequence prior to NICD release. Previously, it was thought that this enzymatic sequence was regulated by modification of the molecular interface between Notch and nicastrin after S2-cleavage (*30*, *31*). Our model does not rule out the contribution of the nicastrin-Notch chemical interface during this process, but our study strongly suggests that the spatial switch is the major regulator of Notch-γ-secretase interaction and signaling, functioning by increasing the concentration of the γ-secretase substrate to the

point that it is efficiently processed by the enzyme. Particularly, our mechanogenetic and the NΔEGF cleavage experiment shown in Figure 1(D-G) and 3, respectively, support the notion that Notch with an intact S2 site is effectively engaged and then processed by γ-secretase when the spatial constraints are removed.

The operating principle of the spatial switch is closely related to another unique feature of Notch receptor: the unusually tall NECD. The functional residues responsible for ligand binding are located near the N-terminus, which protrudes above the crowded cell surface, where they are poised to engage ligands on neighboring cells. Surprisingly, however, it has been also shown that replacing the EGF-like domain repeats with a relatively smaller ligand binding domain (e.g. synNotch) maintains the receptor function (*8*, *37*). Why then does Notch receptor bear such a massive ECD? Our study provides insight into this question, where the large ECD is crucial for its spatial segregation from γ-secretase thereby minimizing nonspecific ligand-independent activation. Low level NICD production was observed even for the Notch variants with a partial EGF truncation ($N\Delta EGF_{1\text{-}25}$), and levels gradually increased upon successive truncations to the NECD size. Our model also explains previous observations where synNotch with a relatively small ECD exhibited significant ligand-independent activation (10-50% of ligand-induced activation) (*28*).

We also show that the size-dependent spatial segregation regulates APP cleavage and Aβ production. It has been previously shown that γ-secretase presenting in different subcellular compartments cleaves APP into diverse Aβ isoforms (*34*, *35*, *38*). Our study shows that, after the ECD cleavage, cadAJ potentiates cell surface processing of APPs within the junction, yielding $A\beta_{40}$ predominantly, while removal of cadAJ produces more $A\beta_{42}$. To establish the relevance of this observation to APP processing will require further investigation in a neuronal system, but our results in model cell lines are consistent with the predominant secretion of Aβ from synapse, where N-cadherin junctions localize (*39*).

The spatial switch is analogous to the kinetic segregation model of T cell activation, where large CD45 phosphatase is excluded from T cell receptor (TCR) immunological synaptic clefts (*10-12*). However, there are several distinct features of the Notch spatial switch compared to the kinetic segregation model. First, unlike the immunological synapse where TCR and CD45 remain constant in size throughout activation, Notch undergoes a dramatic size change during the course of cell surface activation, enabling its dynamic spatial redistribution and sequential proteolysis. Second, the role of cadAJs in Notch signaling is not limited to creating a physical barrier, but also plays the critical role of recruiting γ-secretase to facilitate processing of S2-cleaved Notch at the cell surface. Third and finally, the consequences of size-dependent segregation on signaling are reversed compared to the immunological synapse. While spatial segregation of CD45 enables sustained TCR phosphorylation and downstream signaling, Notch segregation from cadAJs inhibits signal activation. Our result extends the relevance of size-dependent spatial segregation models beyond immune cells (*10-12*, *40*),

supporting the notion that the size-dependent protein segregation can serve as a general mechanism for regulating a broad range of receptor signaling at the cell-cell interface, including Notch and APPs.

Overall, a spatial switching mechanism based on size-dependent protein segregation not only sheds light on the mechanism underlying the sequential proteolysis of Notch and APPs, but also may extend to other receptors processed by γ-secretase. Finally, we anticipate further implications of our work in other areas of research such as providing new design principles for synthetic receptors like synNotch, as well as new therapeutic approaches that target Notch and APP signaling by spatial mutation in cancer and neurodegenerative diseases.

1. S. J. Bray, Notch signalling in context. *Nat. Rev. Mol. Cell Biol.* **17**, 722–735 (2016).

2. R. A. Kovall, B. Gebelein, D. Sprinzak, R. Kopan, The Canonical Notch Signaling Pathway: Structural and Biochemical Insights into Shape, Sugar, and Force. *Dev. Cell*. **41**, 228–241 (2017).

3. A. P. South, R. J. Cho, J. C. Aster, The double-edged sword of Notch signaling in cancer. *Semin. Cell Dev. Biol.* **23**, 458–464 (2012).

4. E. C. Lai, Notch signaling: control of cell communication and cell fate. *Development* **131**, 965–973 (2004).

5. N. Haines, K. D. Irvine, Glycosylation regulates Notch signalling. *Nat. Rev. Mol. Cell Biol.* **4**, 786–797 (2003).

6. H. Takeuchi, R. S. Haltiwanger, Role of glycosylation of Notch in development. *Semin. Cell Dev. Biol.* **21**, 638–645 (2010).

7. X. Wang, T. Ha, Defining single molecular forces required to activate integrin and notch signaling. *Science* **340**, 991–994 (2013).

8. W. R. Gordon *et al.*, Mechanical Allostery: Evidence for a Force Requirement in the Proteolytic Activation of Notch. *Dev. Cell* **33**, 729–736 (2015).

9. D. Seo *et al.*, A Mechanogenetic Toolkit for Interrogating Cell Signaling in Space and Time. *Cell* **165**, 1507–1518 (2016).

10. P. A. van der Merwe, O. Dushek, Mechanisms for T cell receptor triggering. *Nature Reviews Immunology* **11**, 47–55 (2011).

11. M. L. Dustin, J. T. Groves, Receptor signaling clusters in the immune synapse. *Annu. Rev. Biophys.* **41**, 543–556 (2012).

12. J. T. Groves, J. Kuriyan, Molecular mechanisms in signal transduction at the membrane. *Nat. Struct. Mol. Biol.* **17**, 659–665 (2010).

13. M. L. Dustin, A. S. Shaw, Costimulation: Building an Immunological Synapse. *Science* **283**, 649–650 (1999).

14. W. H. Luty, D. Rodeberg, J. Parness, Y. M. Vyas, Antiparallel segregation of notch components in the immunological synapse directs reciprocal signaling in allogeneic Th: DC conjugates. *J. Immunol*. **179**, 819–829 (2007).

15. Y. Narui, K. Salaita, Membrane tethered delta activates notch and reveals a role for spatio-mechanical regulation of the signaling pathway. *Biophys. J.* **105**, 2655–2665 (2013).

16. A. S. Yap, E. M. Kovacs, Direct cadherin-activated cell signaling: a view from the plasma membrane. *J. Cell Biol.* **160**, 11–16 (2003).

17. O. J. Harrison *et al.*, The extracellular architecture of adherens junctions revealed by crystal structures of type I cadherins. *Structure* **19**, 244–256 (2011).

18. C. S. Chen, J. Tan, J. Tien, Mechanotransduction at cell-matrix and cell-cell contacts. *Annu. Rev. Biomed. Eng.* **6**, 275–302 (2004).

19. Z. Kouchi *et al.*, p120 catenin recruits cadherins to gamma-secretase and inhibits production of Abeta peptide. *J. Biol. Chem.* **284**, 1954–1961 (2009).

20. M. Kwak *et al.*, Small, Clickable, and Monovalent Magnetofluorescent Nanoparticles Enable Mechanogenetic Regulation of Receptors in a Crowded Live-Cell Microenvironment. *Nano Lett.* **19**, 3761–3769 (2019).

21. J.-W. Kim, H.-K. Jeong, K. M. Southard, Y.-W. Jun, J. Cheon, Magnetic Nanotweezers for Interrogating Biological Processes in Space and Time. *Acc. Chem. Res.* **51**, 839–849 (2018).

22. V. C. Luca *et al.*, Structural biology. Structural basis for Notch1 engagement of Delta-like 4. *Science* **347**, 847–853 (2015).

23. J. Brasch, O. J. Harrison, B. Honig, L. Shapiro, Thinking outside the cell: how cadherins drive adhesion. *Trends Cell Biol.* **22**, 299–310 (2012).

24. W. J. Polacheck *et al.*, A non-canonical Notch complex regulates adherens junctions and vascular barrier function. *Nature* **552**, 258–262 (2017).

25. I. Indra *et al.*, Spatial and temporal organization of cadherin in punctate adherens junctions. *Proc. Natl. Acad. Sci. U.S.A.* **115**, E4406–E4415 (2018).

26. M. Takeichi, Dynamic contacts: rearranging adherens junctions to drive epithelial remodelling. *Nat. Rev. Mol. Cell Biol.* **15**, 397–410 (2014).

27. W. H. Palmer, W.-M. Deng, Ligand-Independent Mechanisms of Notch Activity. *Trends Cell Biol.* **25**, 697–707 (2015).

28. Z.-J. Yang, Z.-Y. Yu, Y.-M. Cai, R.-R. Du, L. Cai, Engineering of an enhanced synthetic Notch receptor by reducing ligand-independent activation. *Commun. Biol.* **3**, 116 (2020).

29. J. S. Mumm *et al.*, A ligand-induced extracellular cleavage regulates gamma-secretase-like proteolytic activation of Notch1. *Mol. Cell* **5**, 197–206 (2000).

30. S. Shah *et al.*, Nicastrin functions as a gamma-secretase-substrate receptor. *Cell* **122**, 435–447 (2005).

31. D. M. Bolduc, D. R. Montagna, Y. Gu, D. J. Selkoe, M. S. Wolfe, Nicastrin functions to sterically hinder γ-secretase-substrate interactions driven by substrate transmembrane domain. *Proc. Natl. Acad. Sci. U.S.A.* **113**, E509–18 (2016).

32. D. Sprinzak *et al.*, Cis-interactions between Notch and Delta generate mutually exclusive signalling states. *Nature* **465**, 86–90 (2010).

33. R. J. O'Brien, P. C. Wong, Amyloid precursor protein processing and Alzheimer's disease. *Annu. Rev. Neurosci.* **34**, 185–204 (2011).

34. D. J. Selkoe, J. Hardy, The amyloid hypothesis of Alzheimer's disease at 25 years. *EMBO Mol. Med.* **8**, 595–608 (2016).

35. B. De Strooper, E. Karran, The Cellular Phase of Alzheimer's Disease. *Cell*. **164**, 603–615 (2016).

36. M. B. Pepys, Amyloidosis. *Annu. Rev. Med.* **57**, 223–241 (2006).

37. L. Morsut *et al.*, Engineering Customized Cell Sensing and Response Behaviors Using Synthetic Notch Receptors. *Cell*. **164**, 780–791 (2016).

38. G. Yang *et al.*, Structural basis of Notch recognition by human γ-secretase. *Nature* **565**, 192–197 (2019).

39. M. Yuksel, O. Tacal, Trafficking and proteolytic processing of amyloid precursor protein and secretases in Alzheimer's disease development: An up-to-date review. *Eur. J. Pharmacol.* **856**, 172415 (2019).

40. M. H. Bakalar *et al.*, Size-Dependent Segregation Controls Macrophage Phagocytosis of Antibody-Opsonized Targets. *Cell* **174**, 131–142.e13 (2018).

Acknowledgement

The authors thank Drs. Stephen Blacklow (Harvard U.) and C. Miller (King's College London) for the kind gifts of Notch and APP plasmids, respectively. We also thank Dr. Daniel Fletcher (UC Berkeley), Mr. Ari Joffe (UC Berkeley), and Dr. Duaa Al-Rawi (Stanford U.) for helpful discussion. For reagents, technical supports, and discussions we thank the Kim, Cheon, Gartner, and Jun laboratories, as well as the Nikon Imaging Center and Wynton at UCSF. **Funding:** M.K. was supported by a Life Science Research Foundation fellowship as the Shurl and Kay Curci Foundation fellow, and by Burroughs Wellcome Travel Fund. This work was supported by 2020R1A2C4002533 (D.S.) and NRF-2017R1A2B3004198 (H.K.), HI17C0676 from Korean Ministry of Health and Welfare (H.K.), 5R01AG008200 from National Institute on Aging (NIA) and the National Institute of Health (NIH) (N.K.R.), IBS-R026-D1 from IBS (H.K. and J.C.), NRF-2019R1A2C1085712 (Y.H.K.), the UCSF Center for Cellular Construction (an NSF Science and Technology Center, no. DBI-1548297) (Z.J.G.), U01CA244109 from the National Cancer Institute (Z.J.G), 1R01GM112081, 1R01GM126542-01, and R35GM134948 from the National Institute of General Medical Science (NIGMS) and the NIH (Y.J.), and the UCSF Program for Breakthrough Biomedical Research (PBBR) funded in part by the Sandler Foundation (Y.J.). Z.J.G. is a Chan Zuckerberg BioHub Investigator. **Author contributions:** M.K., K.M.S., Z.J.G., and Y.J. conceived the ideas and designed research; M.K. and K.M.S. constructed plasmids, generated cell lines, and performed confocal microscopy. M.K. performed mechanogenetics, truncation study, spatial mutation, immunoblot analysis, reporter cell assay, and APP experiment.

K.M.S. performed Notch exclusion and activation experiments, designed truncation study, wrote custom python image analysis scripts. N.K. performed coarse-grained MD simulation. R.G. generated cadherin-KO cells. W.R.K. performed flotillin staining and mechanogenetic experiment. M.A. and H.L. synthesized magnetic nanoparticles and helped confocal imaging. J.F. and D.S. performed initial proof-of-concept experiment. A.G. and N.K.R. provided anti-PS1 antibodies. H.K., Y.H.K., and J.C. oversaw and supervised CRISPR-Cas9 KO experiment, MD simulation, and magnetic nanoparticle synthesis, respectively. Z.J.G. oversaw and supervised all spatial mapping and mutation experiments. Y.J. oversaw and supervised all aspects of the experiment. M.K. and K.M.S. analyzed data. M.K., K.M.S., Z.J.G., and Y.J. wrote the manuscript. **Competing interests:** The authors declare no competing interest. **Data and materials availability:** All raw images, immunoblot gel images, and analyzed data are available on request. Additional data that support the findings of this study are available from the corresponding author upon reasonable request.

Supplementary Materials

Materials and Methods

Table S1

Figure S1-S13

References (41-73)

Movie S1-S2

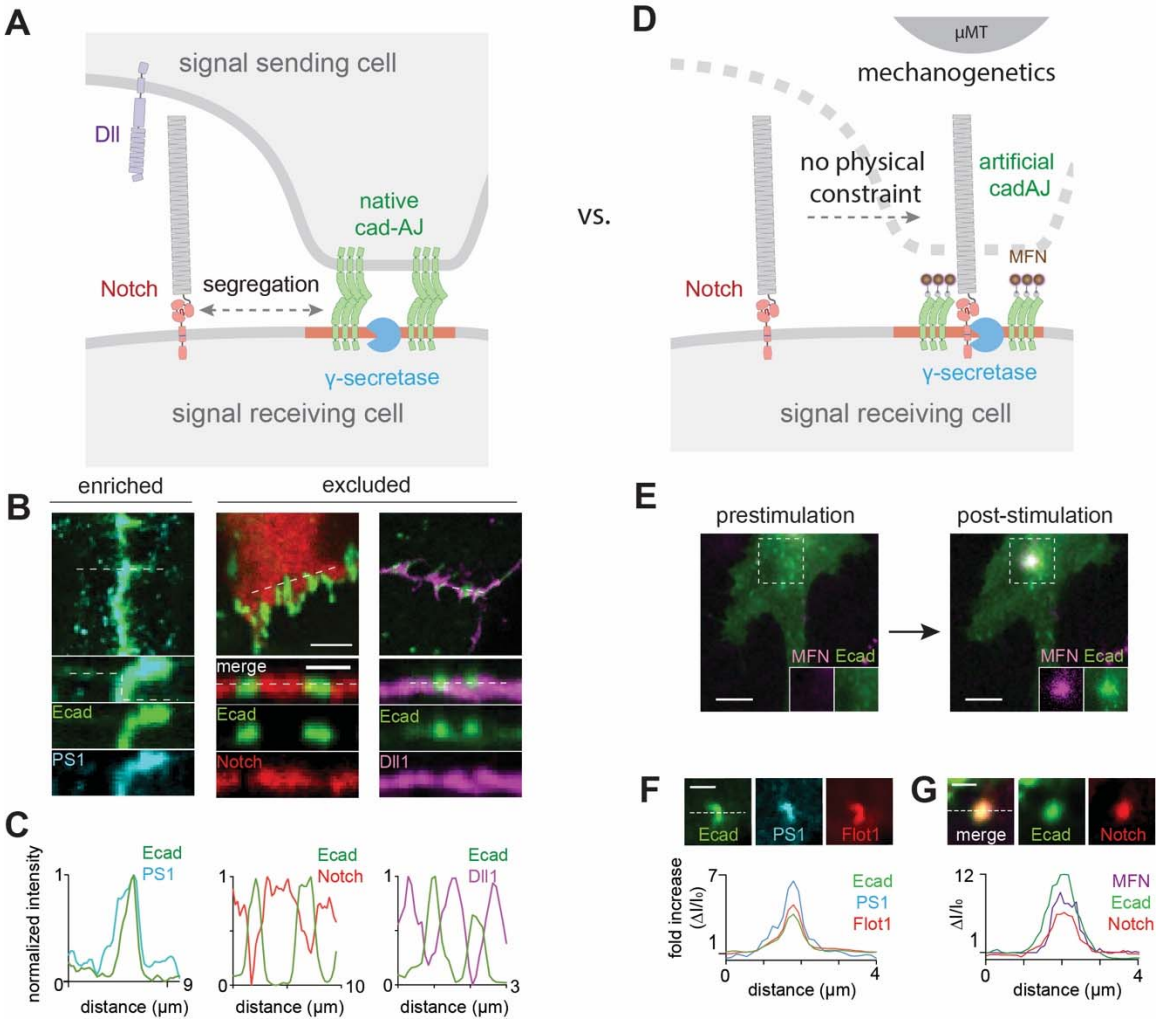

Figure 1. Spatial segregation of Notch receptors and ligands from cadAJs prevents their interactions with γ-secretase. (**A)** A schematic showing spatial distribution of Notch signaling components at the juxtaposed cell-cell interface. (**B)** Representative confocal fluorescence images showing presenilin-1 (PS1), Notch1, and Dll1 distributions relative to E-cadherin-based cadherin junction (cadAJ). (top) A maximum projection image. Scale bar, 5 μm. (bottom) z-resliced images. Scale bar, 3 μm. PS1 was strongly enriched at the cadAJ, whereas Notch1 and Dll1 were segregated from the cadAJ. (**C)** Line profiles quantifying fluorescence from E-cadherin (green), PS1 (cyan), Notch (red), and Dll1 (magenta) along a representative section of the cadAJ (a white dashed line in panel **(B)**, z-resliced images). (**D**) A schematic showing mechanogenetic interrogation of γ-secretase and Notch distribution relative to the artificial cadAJs. Artificial cadAJs were formed by clustering Ecad-GFP labeled with magnetofluorescent nanoparticles (MFNs) by application of an external micromagnetic tweezer (μMT). DAPT was used to inhibit γ-secretase activity during mechanogenetic interrogation of Notch/γ-secretase interaction in absence of the membrane juxtaposition. **(E)** Epifluorescence images showing the formation of an artificial cadAJ by mechanogenetics. After stimulation by μMT, vivid MFN and E-cadherin signals at the magnetic focus were seen, indicating formation of cadAJs. Scale bar, 5 μm. **(F)** Confocal fluorescence images of E-cadherin, PS1, and Flotillin-1 (Flot1) at the artificial cadAJ. Scale bar, 2 μm. Line profiles of E-cadherin, PS1 and Flot1 signals along a white dashed line. $\Delta I/I_0$ represents a fold change relative to nonjunctional membrane signals. **(G)** Confocal fluorescence images showing E-cadherin and Notch distributions at the artificial cadAJs after μMT application. Strong accumulation of Notch signals at the artificial cadAJ was clearly seen. Line profiles of MFN, E-cadherin, and Notch signals along a white dashed line. $\Delta I/I_0$ represents a fold change relative to fluorescence intensity before stimulation. Scale bar, 2 μm.

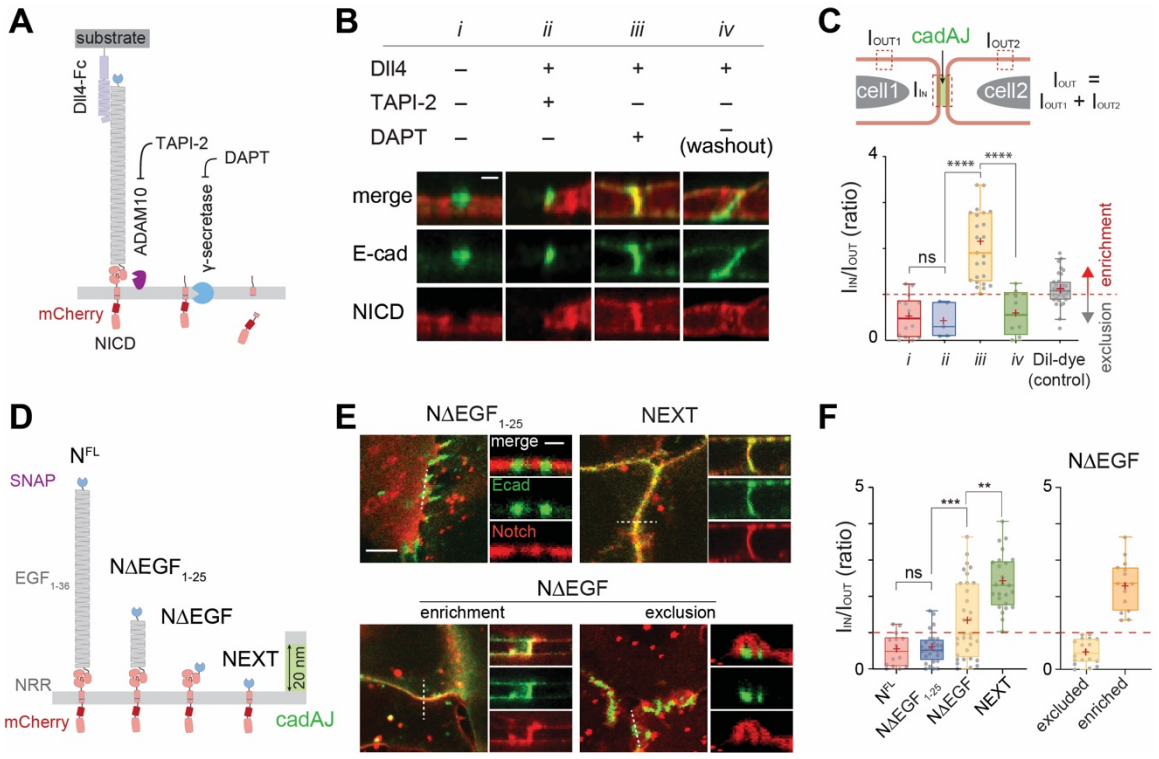

Figure 2. Size-dependent segregation of Notch at the cadAJs controls the proteolytic sequence. (**A**) A schematic to capture the spatial distribution of Notch intermediates during the cell-surface activation pathway. (**B**) Confocal z-resliced images showing Notch distribution (red) relative to cadAJ (green) from the cells without Dll4 activation (i), treated with Dll4 and TAPI2 (ii), treated with Dll4 and DAPT (iii), and washed out to remove DAPT inhibition (iv). Scale bar, 3 μm. (**C**) Quantification of Notch signal enrichment at the cadAJs during the activation. Notch enrichment (I_{IN}/I_{OUT}) is calculated as the ratio of average Notch fluorescence intensity within cadAJs (I_{IN}) and outside cadAJ (I_{OUT}). The enrichment factor of Dil is present as a control showing cadAJ-independent distribution. ****P < 0.0001, ns: non-significant, one-way ordinary ANOVA followed by Tukey's multiple comparison testing. (**D**) Schematics of Notch variants with different truncation lengths, in comparison with the cadAJ intermembrane cleft. (**E**) Confocal fluorescence images showing spatial distribution of the Notch variants (red) relative to the cadAJs (green). To prevent any ligand-independent activation, cells were incubated with TAPI-2 and DAPT. (left) Maximum projections of confocal z-stacks are shown. Scale bar, 5 μm. (right) Confocal z resliced images along the white dashed lines in the maximum projection images. Scale bar, 2 μm. (**F**) Quantification of the enrichment factor (I_{IN}/I_{OUT}) of Notch variants relative to the cadAJs. A box-plot showing binary localization of NΔEGF which are defined as either excluded (yellow) or enriched (orange) is shown on the right. **P < 0.01, ***P < 0.001, ns: non-significant, one-way ordinary ANOVA followed by Tukey's multiple comparison testing. Boxes and whiskers in (**C and F**) indicate the interquartile and the full ranges, respectively. Colored lines and (+) marks indicate median and mean, respectively.

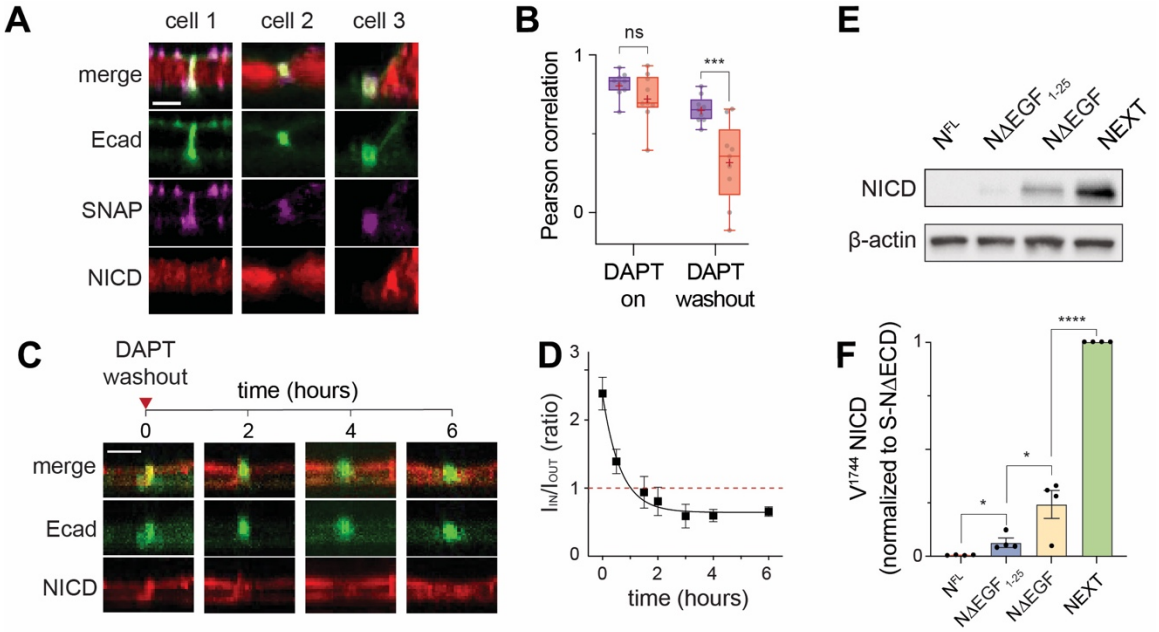

Figure 3. Colocalization of Notch with γ-secretase is sufficient to trigger its proteolysis and signaling, regardless of S2 cleavage or ligand presentation. (**A**) Confocal *z*-resliced images showing the distribution of extracellular SNAP (purple) and intracellular mCherry (red) tags of NΔEGF relative to Ecad-AJs (green) after DAPT removal. Scale bar, 3 μm. (**B**) A box-whisker plot showing Pearson correlation coefficients of extracellular-SNAP (purple) and intracellular-mCherry (red) domains relative to the cadAJs before and after DAPT washout (***P < 0.001; ns, not significant; n = 9 biological replicates; two-tailed unpaired Student's t-test). Boxes and whiskers indicate the interquartile and the full ranges, respectively. Colored lines and (+) marks indicate median and mean, respectively. (**C**)**,** Time series of confocal z-resliced images showing the enrichment of NΔEGF (red) at the cadAJ (green) under DAPT treatment (t = 0), and the dissipation during DAPT washout (t ≥ 2). Scale bar, 3 μm. (**D**) Single-cell traces showing the time-course of the decline of NΔEGF enrichment factor at the cadAJs during DAPT washout (mean ± s.e.m.; n = 4 independent single-cell experiments; see Fig. S6, d-f). (**E and F**) Western blot analyses of cleaved NICD levels in the cells stably expressing N^{FL}, $NΔEGF_{1-25}$, NΔEGF, and NEXT. All cells were transfected with Ecad-GFP and incubated with TAPI2 for 24 hr. β-actin levels represent the loading control. A representative image of immunoblotting (**E**), and quantification (**F**) of cleaved NICD levels. The average intensity of each NICD band relative to respective β-actin band was quantified and then normalized to that of NEXT (mean ± s.d.; n = 4 biological replicates; *P < 0.05, ****P < 0.0001, one-way ANOVA followed by Tukey's multiple comparison test).

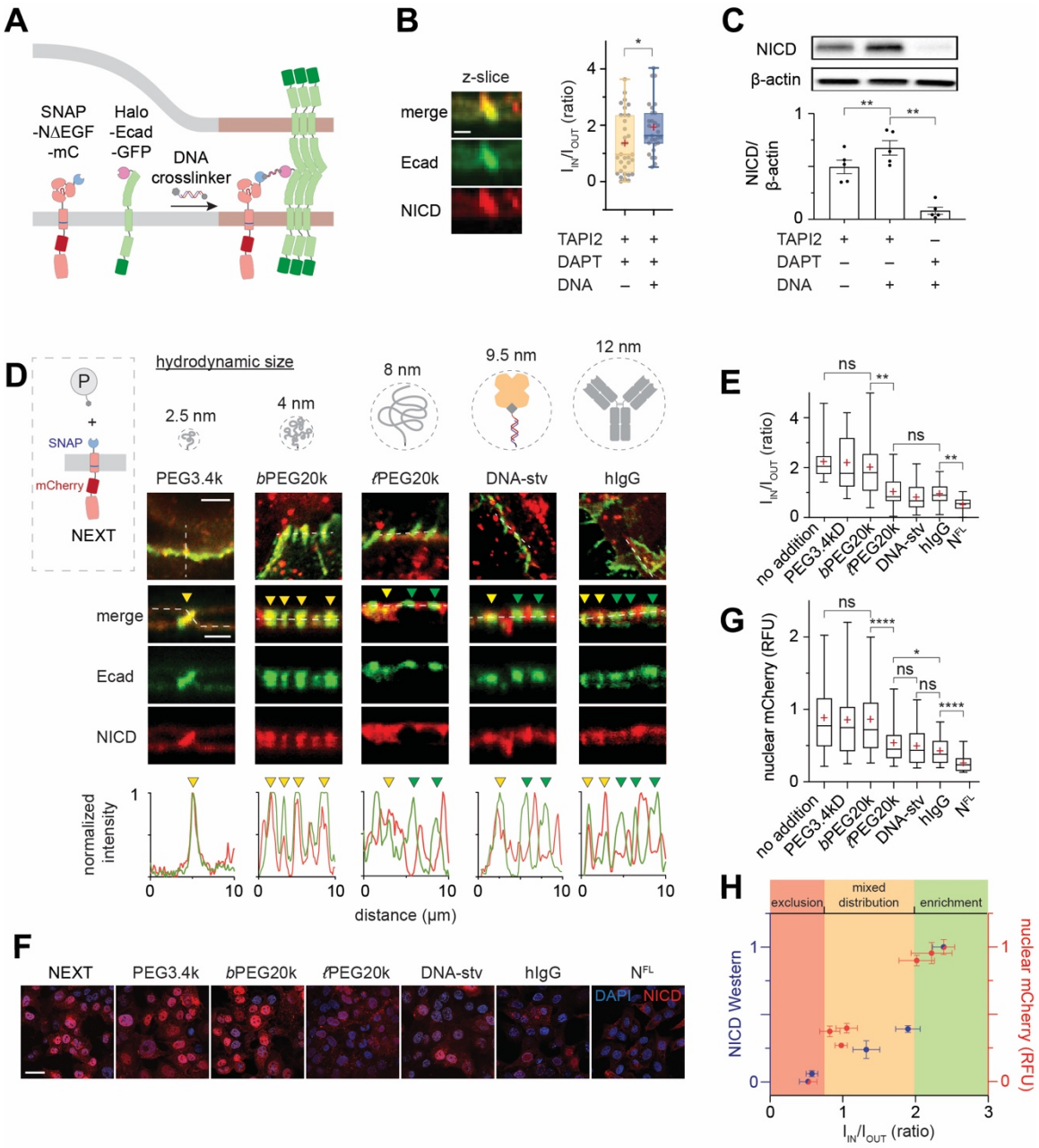

Figure 4. Spatial mutation directs Notch activation, regardless of ligand presentation or S2 cleavage. (A) A schematic describing DNA-mediated crosslinking strategy to enhance NΔEGF localization at the cadAJ. (**B**) Confocal z-resliced images showing intense NΔEGF fluorescence (red) enriched at the cadAJ (green) after the DNA crosslinking. Scale bar, 3 μm. Quantification of enrichment (I_{IN}/I_{OUT}) without (n = 33) with DNA crosslinker treatment (n = 29), indicating an increase in enrichment after the crosslinking (*P < 0.05; two-tailed Mann-Whitney-Wilcoxon test). (**C**) Western blot analyses showing increased S3-cleaved NICD levels in the NΔEGF cells treated with the DNA crosslinker. (top) A representative gel image showing immunoblotting for NICD and β-actin. (bottom) Quantification of cleaved NICD levels. The average intensity of NICD band was normalized to that of β-actin band in each sample. (mean ± s.d.; ** P < 0.01; n = 5 biological replicates; ordinary one-way ANOVA). (**D**) Spatial mutation of NEXT via chemical ligation of macromolecular pendants (denoted as P). 10 μM of BG-modified polymers or proteins were conjugated to the extracellular SNAP tag of NEXT. Cartoons depicting shape and hydrodynamic size of different pendants are shown. Confocal images showing size-dependent spatial mutation of NEXT (red) at the cadAJs (green). The top row shows maximum projection images of the cells treated with the indicated pendants. Scale bar, 5 μm. The middle row shows confocal z resliced images along the white dashed lines in the maximum projection images. Yellow and green arrowheads indicate the cadAJs enriches with and those that excludes Notch,

respectively. Scale bar, 3 μm. The bottom row shows line profiles quantifying fluorescence signals from NEXT (red) and E-cadherin (green) along the white lines in the z-resliced images. Images and line profiles are representative of n ≥ 15 biological replicates. (**E**) Quantification in I_{IN}/I_{OUT} of NEXT with macromolecular pendants (n ≥ 15). (**F**) Confocal fluorescence images of nuclear mCherry signals resulting from nuclear translocation of cleaved NICD (red) in NEXT cells treated with macromolecular pendants. DAPI signals (blue) indicate cell nucleus. Scale bar, 5 μm. **(G)** Quantification of nuclear mCherry fluorescence for NEXT cells treated with the pendants. Cells expressing N^{FL} were used as a negative control. Data shown are from single cells (n ≥ 180) identified in large-area confocal images. **(H)** A plot representing the NICD level of various Notch variants as a function of the enrichment factor (I_{IN}/I_{OUT}, mean ± s.e.m.; n ≥ 15 biological replicates). All Notch variants with different truncation length, DNA crosslinking, or pendant addition used in Figures 2 and 3 were included. The Notch variants showing exclusion, mixed distribution, and enrichment were indicated with red, yellow, and green background colors, respectively (median ± s.e.m.; n ≥ 4 for western blot for NICD levels; n ≥ 180 for nuclear mCherry fluorescence). (**E, G**) Boxes and whiskers indicate the interquartile and the full ranges, respectively. Black lines and (+) marks indicate median and mean, respectively. **P < 0.01; ****P < 0.001; ns, not significant; ordinary one-way ANOVA followed by Tukey's multiple comparison.

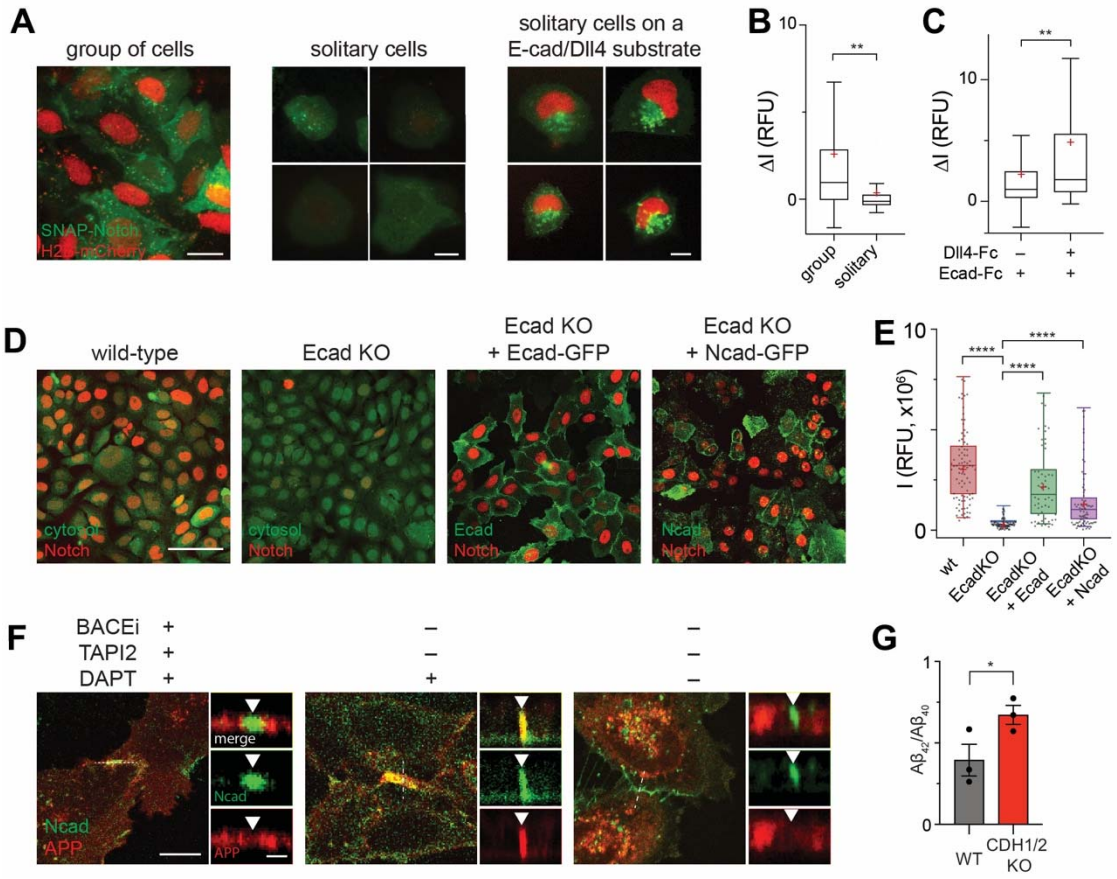

Figure 5. The cadAJ-mediated spatial switch regulates Notch and APP signaling. (**A**) Representative fluorescence images showing Notch activation in U2OS SNAP-N^{FL}-Gal4 reporter cell lines in different cellular environments: Group of cells (left), solitary cells with no prior contact (middle), and solitary cells plated on an Ecad-Fc coated substrate (right). All cells were plated on Dll4-Fc coated substrates. Scale bars, 20 μm (see Supplementary Movie 1, 2). (**B**) Quantification of Notch activation by measuring H2B-mCherry fluorescence changes (intensity at t = 16 hr minus intensity at t = 0 hr) in cells within a group (n = 152), solitary cells (n = 50). (**C**) Quantification of Notch activation in solitary cells cultured on an Ecad-Fc-coated substrate (n = 27) and those cultured without ligands (n = 27). (**D**) Representative confocal images of H2B-mCherry fluorescence in U2OS SNAP-N^{FL}-Gal4 reporter cells (wt), E-cadherin knockout cells (Ecad-KO), Ecad-KO cells with recombinant E-cadherin transfection (Ecad-KO + Ecad), and Ecad-KO cells with N-cadherin transfection (Ecad-KO + Ncad). Cytosol labeled with CMFDA dye was shown for wt and Ecad-KO cells. E-cadherin and N-cadherin were shown for Ecad-KO + Ecad and Ecad-KO + Ncad cells. Scale bar, 100 μm. (**E**) Quantification of Notch activation in the wt, Ecad-KO, Ecad-KO + Ecad, and Ecad-KO + Ncad cells. Data shown are from n ≥ 50 single cells analyzed from two independent experiments. (**F**) (left) Confocal fluorescence maximum projection (left) and z-resliced images of U2OS cells co-expressing Ncad-mCherry (green) and APP-EGFP (red). To capture the APP intermediates, cells were cultured with a combination of α-, β-, and γ-secretase inhibitors. Scale bars, 10 μm (maximum projection) & 3 μm (inset). (**G**) $Aβ_{42}/Aβ_{40}$ ratio measured by ELISA in wild-type cells or CDH1/2 KO cells (mean ± SEM, n = 3, *P< 0.05, two-tailed paired Student's t test). (**B**, **C**, and **E**) Boxes and whiskers indicate the interquartile and full ranges, respectively. Black lines and (+) marks indicate median and mean, respectively. **P < 0.01; ****P < 0.001; ns, not significant; unpaired two-tailed t test in **(B)** and **(C)**; ordinary one-way ANOVA followed by Tukey's multiple comparison in (**E**).